Journal of Materials Chemistry

Cite this: DOI: 10.1039/c2jm31508d

www.rsc.org/materials

PAPER

Sensitization of fullerenes by covalent attachment of a diketopyrrolopyrrole chromophore†

Natalie Banerji,*[a] Mingfeng Wang,[b] Jian Fan,[b] Eneida S. Chesnut,[b] Fred Wudl[b] and Jacques-E. Moser[a]

Received 11th March 2012, Accepted 22nd April 2012
DOI: 10.1039/c2jm31508d

In an effort to develop new materials for organic solar cell applications, we have synthesized triads of 3,6-dithien-2-yl-2,5-dialkylpyrrolo[3,4-*c*]pyrrole-1,4-dione (DTDPP) covalently linked at the nitrogen positions to two [6,6]-phenyl-C_{61}-butyric acid ester (PCB) units *via* alkyl chains of different lengths. We present here the excited-state properties of the compounds in solution, as investigated by (time-resolved) spectroscopy. The absorption spectra of the triads are the composite of the ones recorded with the separate fullerene and DTDPP parent molecules, indicating weak electronic coupling between the sub-units. However, the fluorescence quantum yield drops from 74% in pure DTDPP to <1% in the triads, in both polar *o*-dichlorobenzene (DCB) and non-polar toluene (TOL). According to the energy levels determined by cyclic voltammetry for the parent compounds, charge separation (CS) or excitation energy transfer (EET) could be responsible for the quenching. However, femtosecond-resolved transient absorption (TA) measurements revealed the quenching mechanism to be highly efficient EET from the DTDPP to the PCB moieties. Ultrafast fluorescence spectroscopy showed multiphasic EET dynamics, due to different molecular conformations induced by the flexibility of the alkyl linkers, with time constants ranging from the sub-picosecond to the 100–150 ps scale. The DTDPP chromophore thus acts as a sensitizer (or light-absorbing antenna) to channel light towards the fullerenes, which have low absorbance in the visible range. The ultrafast time scale of the EET leading to fast population of the PCB singlet excited state is particularly interesting for potential use of the systems to increase light harvesting in photovoltaic devices containing fullerenes.

Introduction

In organic bulk heterojunction (BHJ) solar cells, charge carriers are generated at the interface between two blended materials within a solid-state thin film.[1–5] One component acts as the light absorber, electron donor and hole transporter, while the other component (typically a fullerene derivative such as [6,6]-phenyl-C_{61}-butyric acid methyl ester (PCBM)) is the electron acceptor and electron transporter. High power conversion efficiencies of 7–8% can nowadays be achieved in BHJ devices.[6–9]

A challenge in the field is to increase light harvesting, especially since PCBM contributes little due to low absorption in the visible range. The situation is improved if PCBM is replaced by its C_{70} analogue, [6,6]-phenyl-C_{71}-butyric acid methyl ester ($PC_{70}BM$). Another strategy to excite fullerenes with visible light is to covalently attach a sensitizer (antenna chromophore), which strongly absorbs and then transfers the excitation energy to C_{60}.[10–13] Noteworthy are also conjugates of heptamethine cyanines with fullerenes, where light harvesting extends into the near-infrared range and charges can be formed from higher excited states of the cyanine, which thus acts as both antenna and electron donating unit.[14,15] There are a few examples of dye molecules used as sensitizers in BHJ solar cells (the active spectral range is increased due to dye absorption, followed by various energy and charge transfer steps depending on the system).[16–22] However, this typically involves adding the dye as a third component to the donor–acceptor blend. A second challenge to improve BHJ device efficiency is the control of the nanoscale morphology for optimal charge formation and transport. There have been several attempts to achieve this control through well-defined aggregation in covalent single-component systems, where the fullerene acceptor is linked to the donor, instead of having a random blend.[23–34]

The diketopyrrolopyrrole (DPP) chromophore has been primarily known in commercial high-performance pigments used for example as an automotive finish (red car paint).[35,36] More recently, DPP-containing materials, often based on the 3,6-dithien-2-yl-2,5-dialkylpyrrolo[3,4-*c*]pyrrole-1,4-dione (DTDPP) segment, have also attracted attention in optoelectronic

[a]*Institute of Chemical Sciences & Engineering, Ecole Polytechnique Fédérale de Lausanne (EPFL), SB ISIC GR-MO, Station 6, CH-1015 Lausanne, Switzerland. E-mail: natalie.banerji@epfl.ch*
[b]*Center for Polymers and Organic Solids, University of California, Santa Barbara, California 93106-5090, USA*

† Electronic supplementary information (ESI) available: Additional figures. See DOI: 10.1039/c2jm31508d

devices.[37–51] In particular, many conjugated copolymers with DPP groups,[37,38,41,42,46–51] as well as DPP-based small molecules,[43,52–55] have been used in BHJ solar cells. Some covalently linked systems of DPP derivatives with PCBM have also been reported.[39,40,56–58] When charge separation (CS) occurs between the DPP donor and PCBM acceptor, they are interesting candidates for single-component photovoltaic devices.[39,40] On the other hand, the strongly absorbing DPP chromophore can sensitize the fullerene by excitation energy transfer (EET). An attempt has been reported to blend a covalent DPP-sensitized PCBM derivative with a conjugated polymer in a BHJ solar cell.[40]

We report here the excited-state dynamics of two new triads of DTDPP covalently linked at the nitrogen positions to a couple of [6,6]-phenyl-C_{61}-butyric acid ester (PCB) units through alkyl chains of different lengths ($n = 6$, $n = 11$), as shown in Scheme 1 together with the abbreviated names of the compounds. The photophysics of PCB–DTDPPH and PCB–DTDPPU was investigated by steady-state and time-resolved absorption as well as emission spectroscopy. The control compounds PCBM, DTDPPHB and DTDPPU (also shown in Scheme 1) allowed comparing the behavior of the triads to their separate parent moieties. All studies presented here were carried out in solutions of different polarities. They were aimed to determine whether the excited state of the DTDPP moiety in the triads is quenched by the attached PCB units, either by charge separation or by excitation energy transfer. The CS mechanism would make the compounds interesting single-component solar cell materials, while the EET mechanism would provide a means to sensitize PCBM in the visible range.

Experimental part

Materials

PCBM was synthesized and converted to 1-(3-carboxypropyl)-1-phenyl[6,6]-C_{61} (PCBA) according to a reported literature procedure.[59] PCB–DTDPPH was synthesized by reacting PCBA with DT–DPPHB using a modified literature procedure.[60] PCB–DTDPPU was synthesized through an esterification reaction between PCBA and DTDPPU–OH.[59] The *o*-dichlorobenzene (DCB) and toluene (TOL) solvents used for spectroscopy were purchased from Sigma-Aldrich (99.8% anhydrous, sealed) and were used without further purification.

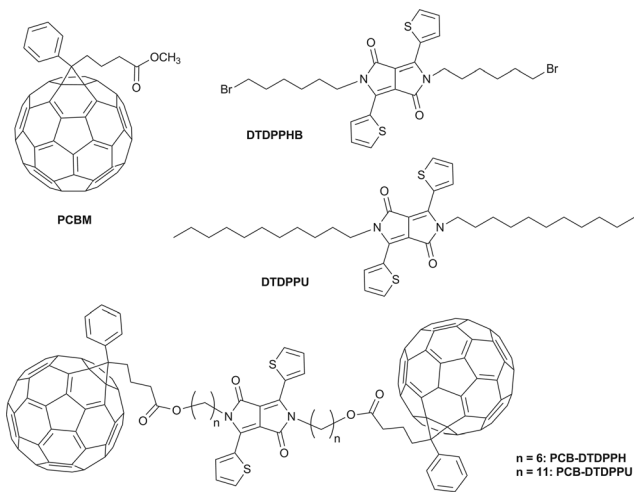

Scheme 1 Molecular structure and abbreviated names of the investigated compounds.

Cyclic voltammetry

The electrochemical measurements were carried out with a Princeton Applied Research Model 263 A Potentiostat/Galvanostat employing Ag/AgCl as the reference electrode, a platinum wire as the counter electrode, and an internal ferrocene/ferrocenium standard.

Steady-state spectroscopy

Absorption spectra were recorded in a 1 cm cuvette on a Cary 5 UV-Vis-IR spectrophotometer. The typical maximum absorbance in the visible range was around 0.1. The same samples very used to record the fluorescence emission spectra on a Fluorolog (Horiba Jobin Yvon, FL 1065) and to determine the fluorescence quantum yields (Φ_f) against Rhodamine 6G in ethanol as a reference ($\Phi_{ref} = 0.99$),[61] using:

$$\Phi_f = \frac{\int F(\lambda)}{\int F_{ref}(\lambda)} \cdot \left(\frac{n}{n_{ref}}\right)^2 \cdot \frac{1 - 10^{A_{ref}}}{1 - 10^{A}} \cdot \Phi_{ref}$$

Here, $\int F(\lambda)$ represents the integral of the sample fluorescence spectrum (in our case in the 513–800 nm range), n is the refractive index of the solvent and A is the absorbance at the excitation wavelength (500 nm for all DTDPP compounds). The quantities indexed with *ref* concern the Rhodamine 6G solution. In order to verify the absence of significant reabsorption effects, we also recorded emission spectra in a highly diluted solution with a 0.025 maximal absorbance and found the same shape. The diluted solutions were also used to record fluorescence excitation spectra, typically at an emission wavelength of 620 nm or 707 nm.

Fluorescence up-conversion spectroscopy

Emission dynamics on the femtosecond time scale were obtained in solution (1 mm cell) using the fluorescence up-conversion setup previously described.[62,63] In brief, the 1000 nm output of a tunable Mai Tai HP (Spectra-Physics) mode-locked Ti:sapphire laser system (100 fs pulse duration, 80 MHz repetition rate) was frequency doubled for sample excitation at 500 nm. The excitation energy was 10 μJ cm^{-2} per pulse and the typical absorbance at the excitation wavelength was 0.3–0.4. The measured sample fluorescence was detected by sum-frequency generation with a delayed gate pulse, then the up-converted signal was dispersed in a monochromator and its intensity measured with a photomultiplier tube. The polarization of the pump beam was at the magic angle (54.7°) relative to that of the gate pulses. Measurements were done at room temperature in ambient conditions. To minimize degradation, the sample cell was constantly rotated during the measurement. Up to 7 scans of the dynamics in the −5 ps to 1000 ps range were averaged at each emission wavelength. The time-resolved emission data were analyzed using the sum of exponential

functions convoluted with a Gaussian-shaped instrument response function (IRF).

Femtoseconds transient absorption spectroscopy

Transient absorption (TA) spectra were recorded using femtosecond pulsed laser pump-probe spectroscopy, for dissolved samples in a 1 mm cell (0.5–0.6 absorbance at the excitation wavelength, same solutions as in the time-resolved emission measurements). The solutions were constantly bubbled with an inert gas during the TA measurements to provide stirring and to remove oxygen. The pump beam (530 nm or 560 nm) was generated with a commercial two-stage non-collinear optical parametric amplifier (NOPA-Clark, MXR) from the 778 nm output of a Ti:sapphire laser system with a regenerative amplifier providing 150 fs pulses at a repetition rate of 1 kHz. The pump power at the sample was at 0.8 mW (530 nm) or 1.2 mW (560 nm) with a spot size diameter of 1–1.5 mm. The probe consisted of a white light continuum (480–750 nm), generated by passing a portion of the 778 nm amplified Ti:sapphire output through a 1 mm thick sapphire plate. The continuum was then intensified by non-collinear optical parametric amplification. The probe intensity was always less than the pump intensity and the spot size was much smaller. The probe pulses were time delayed with respect to the pump pulses using a computerized translation stage.

The probe beam was split before the sample into a signal beam (transmitted through the sample and crossed with the pump beam) and a reference beam. The signal and reference were detected with a pair of 163 mm spectrographs (Andor Technology, SR163) equipped with a 512 × 58 pixels back-thinned CCD (Hamamatsu S07030-0906) and assembled by Entwicklungsbüro Stresing, Berlin. To improve sensitivity, the pump light was chopped at half the amplifier frequency, and the transmitted signal intensity was recorded shot by shot. It was corrected for intensity fluctuations using the reference beam. The transient spectra were averaged until the desired signal-to-noise ratio was achieved (typically 2000–3000 times). The polarization of the probe pulses was at the magic angle relative to that of the pump pulses. All spectra were corrected for the chirp of the white-light probe pulses.

Nanosecond transient absorption spectroscopy

A solution of PCB–DTDPPU in DCB in a 1 cm quartz cell was photoexcited by short light pulses (5 ns FWHM) generated by an optical parametric oscillator pumped by a frequency-tripled Q-switched Nd:YAG laser (Ekspla NT-340). The excitation wavelength was tuned at $\lambda = 500$ nm, where the sample had an absorbance of about 0.3. The pump fluence was of the order of 20 μJ cm^{-2}. The probe light from a Xe arc lamp was passed through filters, various optical elements, the sample, and a grating monochromator, before being detected by a fast photomultiplier tube and recorded by a digital oscilloscope. The kinetic traces were typically averaged over 3000–4000 consecutive laser shots. Prior to the measurement, the solution was de-oxygenated by bubbling argon gas for 20 minutes and the bubbling was maintained during the experiments. To investigate the effect of oxygen on the excited-state behavior, the solution was opened to air for 5 minutes.

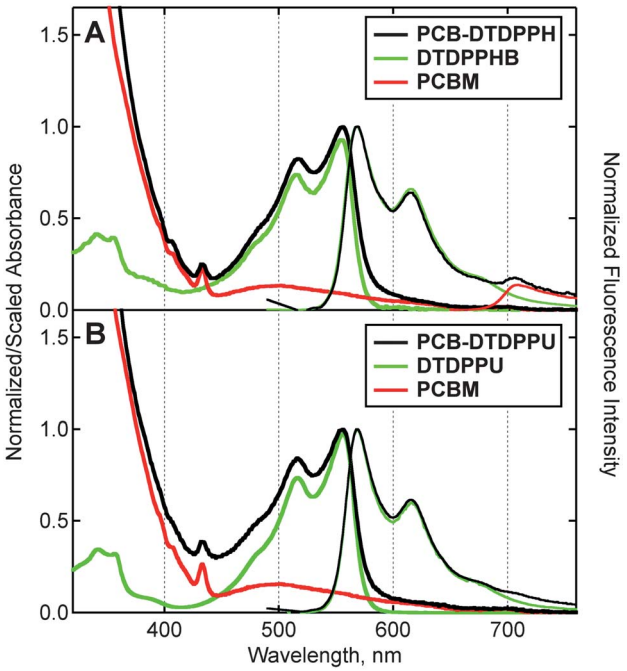

Fig. 1 Steady-state absorption spectra (thick lines, left) and fluorescence emission spectra (thin lines, right) of PCB–DTDPPH (A) and of PCB–DTDPPU (B) in DCB solution. The scaled spectra of the parent compounds (DTDPPHB, DTDPPU and PCBM) in DCB are shown for comparison.

Results and discussion

Steady-state spectra

The normalized absorption spectra of PCB–DTDPPH (hexyl linker, $n = 6$) and PCB–DTDPPU (undecyl linker, $n = 11$) in DCB solution are shown in Fig. 1A and B, respectively, together with the scaled ones of the PCBM and DTDPP parent compounds. Note that the DTDPPU parent compound of PCB–DTDPPU bears pristine alkyl chains, while the DTDPPHB parent compound of PCB–DTDPPH has terminal bromine groups (Scheme 1, for synthetic reasons). The spectra of the two triads are quite similar and they are clearly the sum of the PCBM spectrum and the DTDPP chromophore spectrum, without significant effect of the alkyl chain length. PCBM mainly absorbs below 400 nm with a maximum at 330 nm, but there is a broad absorption band of low oscillator strength around 500 nm, which extends up to 700 nm. DTDPP has an intense, vibronically structured absorption band peaking at 555 nm and a weaker absorption in the 350 nm region. The absence of any shift or change to the individual spectra when the two moieties are linked together points to very weak electronic coupling in the triads, due to the long and non-conjugated linkers.

The steady-state spectra of DTDPPU and PCB–DTDPPU recorded in TOL are shown in Fig. S1 (ESI†), and there is a very slight blue shift of the DTDPP-related visible band (now at 551 nm) compared to DCB (an environment effect because TOL has a lower dielectric constant and refractive index). We note that the photophysics of chemically related triads has recently been independently reported by Karsten *et al.*[57] Those 6T–DPP–PCBC*n* molecules bear six instead of two thiophene groups on

the DPP (three on each side) and the oligothiophene segments are terminated with an additional hexyl chain. Compared to the DTDPP triads presented here, their visible absorption maximum (around 660 nm in DCB solution) is over 100 nm red-shifted, indicating significant differences in the electronic structure.

The fluorescence emission spectra of the DTDPP parent molecules without fullerenes shown in Fig. 1 are similar for the two alkyl chain lengths. With a pronounced vibronic structure, they are close to the mirror image of the first absorption band. The maximum is only very slightly Stokes-shifted, at 568 nm in DCB (565 nm in TOL). The emission spectra of the PCB–DTDPPH and PCB–DTDPPU triads, shown in Fig. 1A and B respectively, were normalized for comparison (they have a much weaker intensity, see below). They are identical to the ones of the parent DTDPP chromophores in the <690 nm region, showing that they are dominated by DTDPP emission. However, there is an additional weak band around 707 nm, which we could assign to emission of the PCB moiety, based on the comparison with the fluorescence spectrum of pure PCBM in DCB (Fig. 1A). In Fig. 2, the fluorescence excitation spectra of PCB–DTDPPH in DCB at different emission wavelengths are shown. The one recorded at 620 nm in the DTDPP emission strongly resembles the absorption spectrum of pristine DTDPPHB, without contribution from the fullerenes. It can be concluded that it stems entirely from excitation of this moiety and that there is no EET in the direction from PCB to DTDPP. On the other hand, the excitation spectrum recorded at 707 nm, where PCB contributes to the emission, matches the absorption spectrum of PCB–DTDPPH with equal contributions from the fullerene and DTDPP moieties. This shows that emission at 707 nm occurs no matter which part of the molecule is excited. The result implies that the PCB emitting at 707 nm is not only directly excited, but also *via* EET from the DTDPP chromophore.

Steady-state and time-resolved fluorescence quenching

The fluorescence quantum yields of the investigated compounds are summarized in Table 1. The DTDPP control compounds both have a high emission yield of about 74% in solution. This drops to <1% when the PCB units are attached in the triads. The quenching is more efficient (lower Φ_f) in PCB–DTDPPH compared to PCB–DTDPPU, because of the shorter linker and ensuing smaller distance between the quenching partners (even through space as explained below). Both CS and EET can be envisaged as a quenching mechanism. Since the strong quenching occurs in both medium polar DCB and in weakly polar TOL, EET appears to be more probable. Indeed, the lesser stabilization of charges in a non-polar medium should reduce the efficiency of CS. On the contrary, the fluorescence quantum yield is lower (about half) in TOL compared to DCB.

Table 1 Fluorescence quantum yields of the investigated compounds

Sample	Solvent	Φ_f
DTDPPHB	DCB	0.74
DTDPPU	DCB	0.73
PCB–DTDPPH	DCB	0.002
PCB–DTDPPH	TOL	0.001
PCB–DTDPPU	DCB	0.007
PCB–DTDPPU	TOL	0.004

The fluorescence time profiles recorded at the 568 nm emission maximum following 500 nm excitation are compared in Fig. 3A for the parent chromophores (DTDPPHB and DTDPPU) and the triads (PCB–DTDPPH and PCB–DTDPPU) in DCB solution. In spite of the bromine groups attached only to DTDPPHB, the two pristine DTDPP molecules show almost the same emission dynamics. This is characterized by a fast rise (0.5 ps with the hexyl chain, 1.3 ps with the undecyl chain), which we assign to vibrational relaxation, followed by a slow 5 ns decay in both compounds. For DTDPPHB, we recorded the dynamics at various emission wavelengths from 586 nm to 707 nm (Fig. S2, ESI†) and found no significant differences. This confirms that,

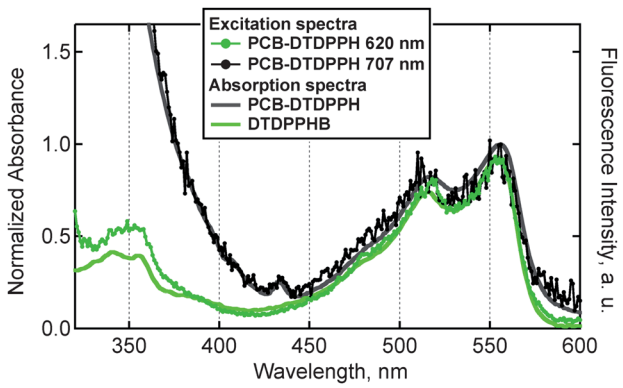

Fig. 2 Fluorescence excitation spectra of PCB–DTDPPH in DCB recorded at 620 nm and 707 nm (lines with markers). The absorption spectra of PCB–DTDPPH and of DTDPPHB in DCB are shown for comparison (smooth lines).

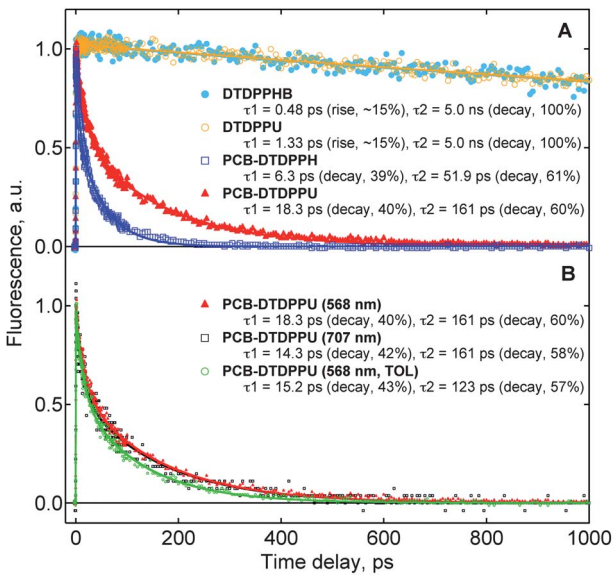

Fig. 3 (A) Femtosecond fluorescence time profiles of the molecules shown in the legend dissolved in DCB, recorded at 568 nm following excitation at 500 nm. (B) Femtosecond fluorescence time profiles of PCB–DTDPPU in DCB at 568 nm (red triangles) and at 707 nm (black boxes), as well as of PCB–DTDPPU in TOL at 568 nm (green circles). The solid lines are the best biexponential fits (convoluted with a 140 fs IRF).

apart from the fast vibrational relaxation, there is no significant excited-state relaxation (geometrical, solvation) leading to any spectral dynamics, in agreement with the small Stokes shift and mirror-symmetry of the steady-state spectra (Fig. 1).

In the presence of the PCB moieties in the triads, the fluorescence of the DTDPP chromophore at 568 nm decays much faster than 5 ns (Fig. 3A, in DCB). In accord with the lower fluorescence quantum yield, the quenching rate is increased in PCB–DTDPPH (shorter linker) compared to PCB–DTDPPU. For both triads, the quenching does not occur with a single time constant, but shows biexponential decay (PCB–DTDPPH: 39% 6.3 ps, 61% 51.9 ps; PCB–DTDPPU: 40% 18.3 ps, 60% 161 ps). It is probable that there are additional quenching components faster than the 140 fs time resolution of the experiment. Although this is not a quantitative measure due to small changes in alignment, the initial ("time zero") intensity of the fluorescence up-conversion signal was indeed 3–4 times smaller in the triads compared to the unlinked DTDPP compounds, although similar chromophore concentrations (similar absorbances) were used.

The multiphasic quenching can be explained by the flexibility of the alkyl chains linking the PCB and DTDPP moieties, allowing for a variety of conformations and thus distances of the quenching partners in solution. Quenching most probably occurs through space when the linker folds and the PCB quencher comes close to the chromophore, rather than through the bonds of the non-conjugated alkyl chains. Nevertheless, the fullerenes are on average restricted to a certain distance from the DTDPP by the length of the alkyl chains. The flexibility of the linker allows for them to diffuse within a range, which is smaller for a shorter linker. Depending on the conformation at the moment of excitation, it will take more or less time for the fullerene to diffuse to a quenching distance, leading to the various time constants. As the average through-space distance of the moieties is longer in PCB–DTDPPU, the quenching is slower.

Finally, Fig. 3B compares the fluorescence decay of PCB–DTDPPU in DCB and TOL at 568 nm. As expected from the fluorescence quantum yields (Table 1), the quenching is slightly faster in TOL (43% 15.2 ps, 57% 123 ps). The lower viscosity of TOL, allowing faster diffusion of the fullerene moiety, explains this result. In Fig. 3B, the emission dynamics of PCB–DTDPPU in DCB is also compared at 568 nm and 707 nm, revealing no significant difference. At the longer wavelength, we expected a contribution of PCB emission (see Fig. 1), which might have appeared as a slow component in the case of EET to the fullerene moiety. The oscillator strength of the PCB emission is however too low to make such an observation.

Determination of the quenching mechanism by femtosecond TA spectroscopy

The HOMO and LUMO levels of PCBM and of the DTDPP chromophore are depicted in Fig. 4 (estimated from cyclic voltammetry of PCBM and of DTDPPHB in solution, see Fig. S3 of the ESI†). Energetically speaking, the excited DTDPP chromophore can transfer either excitation energy (green dotted arrows) or an electron (red smooth arrow) to PCBM. Given the small electronic coupling between the two moieties, EET should proceed *via* the Förster mechanism (FRET), which implies a simultaneous relaxation of the photoexcited donor and

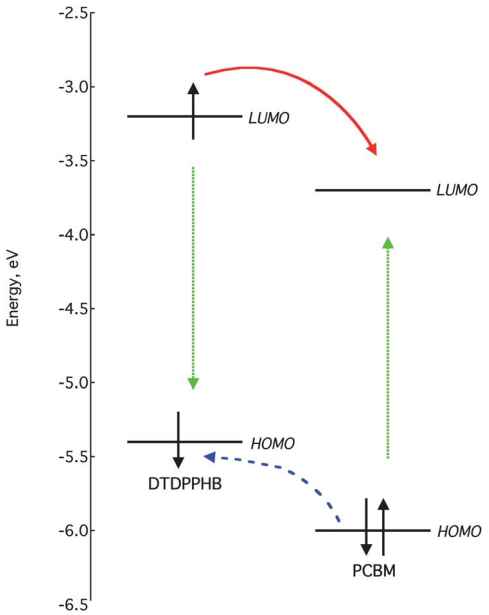

Fig. 4 HOMO and LUMO levels of PCBM and DTDPPHB as estimated from electrochemistry. The possible pathways of EET (green dotted arrows) and CS (red smooth arrow) from the excited state of the DTDPP chromophore are also indicated, as well as hole transfer (HT) from PCBM to DTDPP (blue dashed arrow).

excitation of the acceptor due to Coulomb interactions of their transition dipole moments. This mechanism requires an overlap of the acceptor absorption spectrum with the emission spectrum of the donor, which is the case for PCBM and DTDPP (Fig. 1). EET is also favored by the high fluorescence quantum yield of the DTDPP chromophore (Table 1). It should be noted that hole transfer from the excited state of PCBM to DTDPP is also possible (blue dashed arrow, Fig. 4).

In order to unambiguously determine the quenching mechanism(s) occurring in the excited state of the triads, we carried out TA spectroscopy. The femtosecond-resolved TA spectra following 560 nm excitation of PCB–DTDPPU and its DTDPPU parent compound in DCB are shown in Fig. 5. There is a broad and structured negative band in the 480–660 nm range. By comparison to the ground-state absorption spectrum and the stimulated emission spectrum (steady-state emission multiplied by λ^4) of the samples (shown in black), this TA band can be assigned to a combination of DTDPP ground-state bleach (GSB) and DTDPP stimulated emission (SE). We attribute the positive TA band above 660 nm to singlet excited-state absorption (ESA) from the DTDPP chromophore. For DTDPPU (Fig. 5A), there is no significant evolution of the spectral features in the shown temporal window, in agreement with the long-lived excited state observed in the time-resolved emission measurements.

On the other hand, the GSB, SE and ESA bands decay in the triads, because the excited state of the DTDPP moiety is quenched by the attached fullerenes (Fig. 5B). A weak positive signal extending throughout the TA spectrum (from 480 nm to 750 nm) appears at longer time delays due to the signature of the quenching product. Its intensity stays constant up to the longest measured 1 nanosecond time delay. In Fig. 5C, the 1 ns spectrum of PCB–DTDPPU (quenching product and a weak contribution

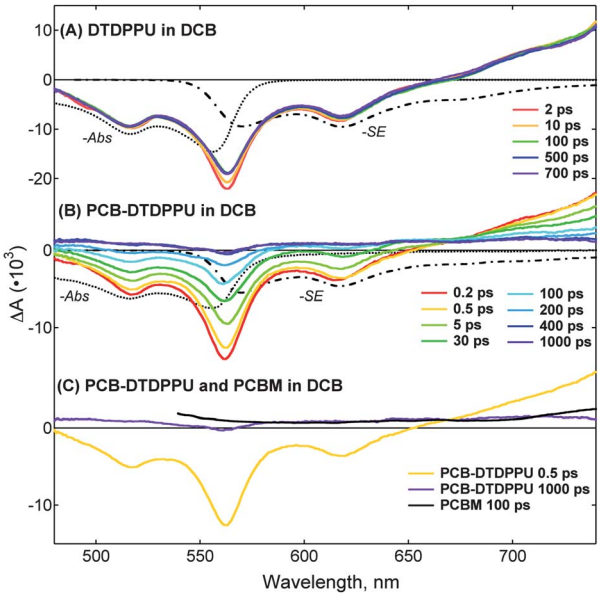

Fig. 5 Femtosecond transient absorption spectra at various time delays after 560 nm excitation of (A) DTDPPU in DCB, (B) PCB–DTDPPU in DCB and (C) both PCB–DTDPPU and PCBM in DCB (520 nm excitation). The negative steady-state absorption spectra (−Abs) and stimulated emission spectra (−SE, steady-state emission multiplied by λ^4) are shown for comparison as dotted and dashed black lines, respectively.

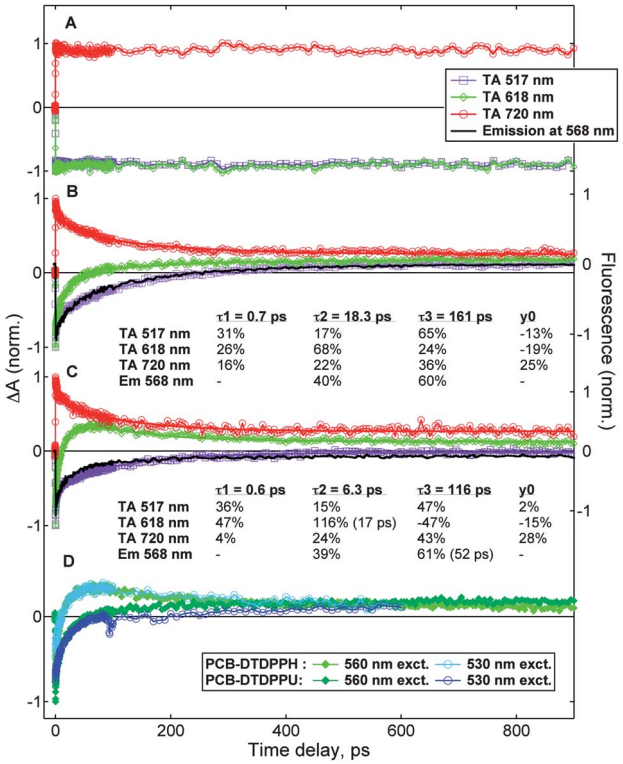

Fig. 6 Femtosecond transient absorption dynamics at various spectral positions after 560 nm excitation of (A) DTDPPU in DCB, (B) PCB–DTDPPU in DCB and (C) PCB–DTDPPH in DCB. Solid lines represent multiexponential global fits; the obtained parameters are shown in the inset tables. The smooth black lines in (B) and (C) are the scaled 568 nm emission dynamics recorded for the corresponding samples by fluorescence up-conversion spectroscopy. In (D), the dynamics of the two triads in DCB at 618 nm are compared for 530 nm and 560 nm excitation.

of DTDPP GSB) is compared to the singlet ESA of pure PCBM (recorded at 100 ps for a pure PCBM solution in DCB excited at 520 nm). It is clear that the spectrum of the quenching product in PCB–DTDPPU is due to the singlet excited state of the PCB moieties. This allows us to definitely assign the quenching mechanism in the triad to EET from the excited DTDPP chromophore to the fullerenes. Assuming that the singlet excited state of the chromophore is populated with a quantum yield of unity following excitation, the quantum yield of the singlet EET (Φ_{EET}) can be estimated from the fluorescence quantum yields of the DTDPPU parent molecule (not quenched) and the PCB–DTDPPU triad (quenched):

$$\Phi_{EET} = 1 - \frac{\Phi_f^{PCB\text{-}DTDPPU}}{\Phi_f^{DTDPPU}}$$

Thus, the singlet excited state of the PCB moiety in PCB–DTDPPU is populated by EET with a quantum yield of 99.0% in DCB and of 99.5% in TOL. The TA spectra for the compounds with the shorter alkyl chains (DTDPPHB and PCB–DTDPPH in DCB) are depicted in Fig. S4 of the ESI†. Essentially, the same observations as with the longer linker can be made, evidencing EET as the quenching mechanism. Here, the quantum yield of the energy transfer process is 99.7% in DCB and 99.9% in TOL. The only differences compared to PCB–DTDPPU are that the quenching is faster (slightly more efficient due to the shorter linker) and that the signature of the quenching product slightly decays at long time delays, instead of remaining constant.

This is clearer in the time profiles of the TA bands shown for DTDPPU, PCB–DTDPPU and PCB–DTDPPH in DCB in Fig. 6. As expected, the dynamics of the GSB at 517 nm, of the SE at 618 nm and of the ESA at 720 nm are long-lived for DTDPPU (Fig. 6A). In the triads (Fig. 6B and C), the negative GSB signal decays and is replaced by the weakly positive signal of the PCB singlet excited state (EET quenching product). The scaled emission time profiles from the fluorescence up-conversion measurements at 568 nm are also shown in Fig. 6 for comparison and match well the GSB dynamics (if the offset due to the quenching product is discarded). This indicates that the quenching of the DTDPP excited state is concomitant with ground state recovery in the chromophore, which is further evidence for the EET mechanism. In the triads, the dynamics at 720 nm (mainly ESA of DTDPP at early times) mirrors the GSB dynamics and ends in a plateau due to ESA from the fullerenes. The decay of the negative SE signature at 618 nm appears however faster than the one of the GSB, although a similar dynamics is expected in the case of EET without a reactional intermediate. The effect is probably due to the strong overlap at this wavelength of the negative (decaying) SE signal and the positive (growing) PCBM ESA signal. We also note that there is a slow decay (116 ps time constant) of the quenching product at 618 nm only in PCB–DTDPPH (Fig. 6C and D). This could again be a consequence of overlapping TA bands, since a similar decay is observed at 720 nm. It could also be an indication that the singlet excited PCB moieties live less long in the compound

with the shorter alkyl chain, due to intersystem crossing (ISC) to the triplet state or some back-quenching mechanism with the DTDPP unit.

For PCB–DTDPPH and PCB–DTDPPU in DCB, the TA dynamics at the three wavelengths shown in Fig. 6 were globally analyzed with the sum of three exponential functions (because the quenching is multiphasic as discussed before) and an offset (due to the long-lived excited state of the fullerenes populated by EET). The time constants and amplitudes at the different wavelengths are shown in the inset tables of Fig. 6. For PCB–DTDPPU (Fig. 6B), the same two time constants as in the emission decay (Fig. 3) were found, together with an additional fast 0.7 ps component. The fast component (0.6 ps) is also present in PCB–DTDPPH; it could be due to quenching or to an artifact such as cross-phase modulation in the TA experiments. In PCB–DTDPPH, the third time constant (116 ps) was found to be longer than the 52 ps time constant from the fluorescence up-conversion data, possibly due to overlapping decay of the excited fullerene quenching product. Finally, we also repeated the TA experiments with excitation at 530 nm (the 618 nm dynamics is compared for 530 nm and 560 nm excitation in Fig. 6D for both triads). There is no observable effect of the excitation wavelength and the data simply confirm that quenching is faster with the shorter hexyl linker, no matter where the sample is excited.

Population of the triplet state at long time delays (nanosecond TA spectroscopy)

An interesting observation in Fig. 5B is that there remains some GSB of the DTDPP moiety after 1 ns for the PCB–DTDPPU triad in DCB, although the time-resolved emission data (Fig. 3C) show that the excited state of the DTDPP unit is completely quenched for this sample at this time delay. This unexpected behavior at long times means that a small fraction of the DTDPP population is neither in the ground state (where it should be following EET to the fullerenes) nor the excited state. It could for example be in the triplet or charge separated state instead. In principle, some CS from the excited state of DTDPP can occur in parallel to EET, or the CS state can be populated after EET to the PCB moiety, by hole transfer from the excited state of the fullerene (Fig. 4). Such a behavior has previously been observed in a triad where two fullerene units were attached to a DTDPP chromophore *via* the thiophenes (not *via* the nitrogen atoms as here).[56] However, the absorption of the DTDPP radical cation (around 610 nm and 855 nm in DCB) could in this case clearly be evidenced in the femtosecond TA spectra. For the triads presented here, there is no sign of any significant DTDPP cation absorption above 600 nm in the TA spectra after the initial quenching (Fig. 5 and S4†). The positive TA signature at 1 ns seems to arise predominantly from singlet ESA of the PCB moieties, so that the remaining DTDPP GSB at this time delay is more probably due to population of its triplet state, rather than to CS.

The triplet state of DTDPP in DCB solution absorbs mainly above 750 nm (maximum at 861 nm),[56] so that it is outside the spectral window of our femtosecond TA experiments (Fig. 5). In order to verify that the DTDPP triplet state is populated at long time delays in the triads, we recorded nanosecond TA dynamics of PCB–DTDPPH in DCB solution. We found indeed a negative

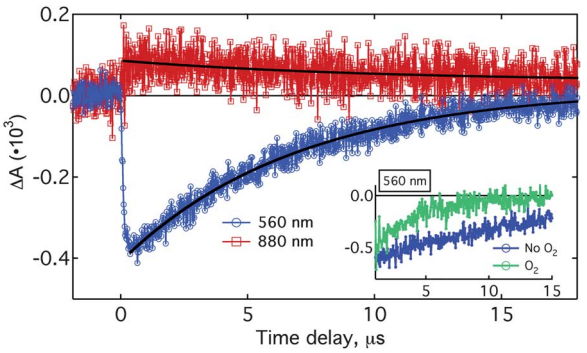

Fig. 7 Nanosecond TA dynamics recorded at different wavelengths for PCB–DTDPPH in DCB solution following excitation at 500 nm. Unless stated otherwise, oxygen was removed from the solution.

signature due to the DTDPP GSB at 560 nm and a positive signature due to the triplet absorption at 880 nm, which extend into the microsecond regime (Fig. 7). The GSB decayed faster in the presence of oxygen, confirming the assignment to the triplet state (inset of Fig. 7). The presence of fullerene is necessary to populate the triplet state of the DTDPP chromophore, since direct intersystem crossing from the singlet excited state occurs in negligible yield.[56,57] In the previously reported triad with fullerenes attached to the thiophene groups of DTDPP, the triplet state was formed upon charge recombination.[56] This mechanism can be excluded here due to the absence of charges. For other 6T–DPP–PCBC*n* triads recently reported by Karsten *et al.* and related to our systems,[57] a shuttling mechanism in the excited state was suggested. Following EET from the 6T–DPP to the PCB units, there is near-quantitative ISC to the fullerene triplet state and then back-EET to the triplet state of 6T–DPP. We conclude that a similar mechanism probably occurs here for PCB–DTDPPH and PCB–DTDPPU in solution.

Summary and conclusions

We reported here the synthesis and solution-state photophysical characterization of two triads consisting of the DTDPP chromophore covalently linked to two fullerene (PCB) units *via* hexyl ($n = 6$) or undecyl ($n = 11$) chains. Although there is very weak electronic coupling between the two moieties, the excited state of the chromophore is very efficiently quenched by the fullerenes and the fluorescence quantum yield drops from 74% in pristine DTDPP to <1% in the triads, in both polar DCB and non-polar TOL solution. Ultrafast fluorescence up-conversion spectroscopy showed multiphasic quenching dynamics, which can be explained by the flexibility of the alkyl chains linking the PCB and DTDPP moieties. Depending on the conformation at the moment of excitation, it will take more or less time for the fullerene to diffuse to a through-space quenching distance, leading to the various time constants. As the average distance of the partners is longer in PCB–DTDPPU, the quenching was found to be slower. It is on the other hand faster in less viscous TOL compared to DCB (faster diffusion). In principle, PCB can act as an electron or energy acceptor in the investigated systems (judging from the frontier molecular orbital levels). Our femtosecond TA experiments revealed however that highly efficient

singlet EET (quantum yield ≥99%) is the predominant quenching mechanism in solution. On the long time scale, the excitation energy is transferred back to the triplet state of the DTDPP chromophore, following quantitative intersystem crossing in the PCB units. We could not evidence any formation of charges for the two triads in solution.

Concerning potential applications of the investigated triads in organic solar cells, the compounds seem *a priori* not suitable for use as a single-component BHJ material, because of the absence of charges. It should however be noted that the quenching mechanism in covalently linked PCBM systems tends to switch from EET in solution to CS in the solid state (thin films).[23,40] This behavior was observed for related 6T–DPP–PCBC*n* triads, which were used as linked electron donor–acceptor materials in single component BHJ devices.[40] We are currently investigating the solid-state properties of PCB–DTDPPH and PCB–DTDPPU, but preliminary measurements showed negligible photocurrent for those materials. Nevertheless, the results presented here indicate that the triads have potential use as antenna systems in which the PCB units are sensitized for high absorption in the visible range by the attached DTDPP chromophore. The multiphasic EET is ultrafast, with time constants ranging from the sub-picosecond to the 100–150 ps scale. This means that the fullerene excited state is populated quickly after initial photoexcitation of the DTDPP moiety. By adding an appropriate electron donor, CS from the excited PCBM can then in principle lead to the charge formation necessary in photovoltaic devices. From our measurements it is clear that the singlet excited state of the PCB units survives at least for one nanosecond. Since CS in BHJ solar cells is typically much faster than this,[64–66] the population of the PCB triplet state and subsequently DTDPP triplet state at long time delays should not be in competition with charge formation. Since low light harvesting by the fullerene in BHJ solar cells reduces photovoltaic efficiency, the use of a DTDPP sensitizer is a strategy definitely worth exploring.

Acknowledgements

NB thanks the Swiss National Science Foundation for funding (NCCR MUST program and Ambizione Fellowship PZ00P2_136853). NB is grateful to Professor Eric Vauthey for use of the fluorescence up-conversion setup, to Dr Robin Humphry-Baker for use of the Fluorolog, and to Jelissa Dejonghe, Arianna Marchioro, Elham Ghadiri and Romain Letrun for useful discussions regarding the apparatuses. MW thanks the Natural Sciences and Engineering Research Council of Canada for the support through a Postdoctoral Fellowship.

Notes and references

1 A. J. Heeger, N. S. Sariciftci and E. B. Namdas, *Semiconducting and Metallic Polymers*, Oxford University Press Oxford, UK, 2010.
2 B. C. Thompson and J. M. J. Frechet, *Angew. Chem., Int. Ed.*, 2008, **47**, 58–77.
3 C. J. Brabec, *Sol. Energy Mater. Sol. Cells*, 2004, **83**, 273–292.
4 C. J. Brabec, N. S. Sariciftci and J. C. Hummelen, *Adv. Funct. Mater.*, 2001, **11**, 15–26.
5 G. Yu, J. Gao, J. C. Hummelen, F. Wudl and A. J. Heeger, *Science*, 1995, **270**, 1789–1791.
6 J. P. Lu, T. Y. Chu, S. Beaupre, Y. G. Zhang, J. R. Pouliot, S. Wakim, J. Y. Zhou, M. Leclerc, Z. Li, J. F. Ding and Y. Tao, *J. Am. Chem. Soc.*, 2011, **133**, 4250–4253.
7 A. J. Heeger, Y. M. Sun, C. J. Takacs, S. R. Cowan, J. H. Seo, X. Gong and A. Roy, *Adv. Mater.*, 2011, **23**, 2226–2230.
8 L. P. Yu, Y. Y. Liang, Z. Xu, J. B. Xia, S. T. Tsai, Y. Wu, G. Li and C. Ray, *Adv. Mater.*, 2010, **22**, E135–E138.
9 H. Y. Chen, J. H. Hou, S. Q. Zhang, Y. Y. Liang, G. W. Yang, Y. Yang, L. P. Yu, Y. Wu and G. Li, *Nat. Photonics*, 2009, **3**, 649–653.
10 C. C. Hofmann, S. M. Lindner, M. Ruppert, A. Hirsch, S. A. Haque, M. Thelakkat and J. Kohler, *J. Phys. Chem. B*, 2010, **114**, 9148–9156.
11 G. Bottari, G. de la Torre, D. M. Guldi and T. Torres, *Chem. Rev.*, 2010, **110**, 6768–6816.
12 C. van der Pol, M. R. Bryce, M. Wielopolski, C. Atienza-Castellanos, D. M. Guldi, S. Filippone and N. Martin, *J. Org. Chem.*, 2007, **72**, 6662–6671.
13 L. Sanchez, N. Martin, E. Gonzalez-Cantalapiedra, A. M. Echavarren, G. M. A. Rahman and D. M. Guldi, *Org. Lett.*, 2006, **8**, 2451–2454.
14 C. Villegas, E. Krokos, P. A. Bouit, J. L. Delgado, D. M. Guldi and N. Martin, *Energy Environ. Sci.*, 2011, **4**, 679–684.
15 P. A. Bouit, F. Spanig, G. Kuzmanich, E. Krokos, C. Oelsner, M. A. Garcia-Garibay, J. L. Delgado, N. Martin and D. M. Guldi, *Chem.–Eur. J.*, 2010, **16**, 9638–9645.
16 H. C. Hesse, J. Weickert, C. Hundschell, X. Feng, K. Muellen, B. Nickel, A. J. Mozer and L. Schmidt-Mende, *Adv. Energy Mater.*, 2011, **1**, 861–869.
17 S. Honda, H. Ohkita, H. Benten and S. Ito, *Chem. Commun.*, 2010, **46**, 6596–6598.
18 B. P. Rand, C. Girotto, A. Mityashin, A. Hadipour, J. Genoe and P. Heremans, *Appl. Phys. Lett.*, 2009, **95**, 173304.
19 S. Honda, S. Yokoya, T. Nogami, H. Ohkita, H. Benten and S. Ito, *Polym. Prepr. (Am. Chem. Soc., Div. Polym. Chem.)*, 2009, **50**, 804–810.
20 A. A. Bakulin, S. A. Zapunidy, M. S. Pshenichnikov, L. P. H. M. van and D. Y. Paraschuk, *Phys. Chem. Chem. Phys.*, 2009, **11**, 7324–7330.
21 J. Peet, A. B. Tamayo, X. D. Dang, J. H. Seo and T. Q. Nguyen, *Appl. Phys. Lett.*, 2008, **93**, 163306.
22 A. Ltaief, C. R. Ben, A. Bouazizi and J. Davenas, *Mater. Sci. Eng., C*, 2006, **26**, 344–347.
23 N. Banerji, J. Seifter, M. F. Wang, E. Vauthey, F. Wudl and A. J. Heeger, *Phys. Rev. B: Condens. Matter Mater. Phys.*, 2011, **84**, 075206.
24 R. C. Hiorns, E. Cloulet, E. Ibarboure, A. Khoukh, H. Bejbouji, L. Vignau and H. Cramail, *Macromolecules*, 2010, **43**, 6033–6044.
25 F. Ouhib, A. Khoukh, J. B. Ledeuil, H. Martinez, J. Desbrieres and C. Dagron-Lartigau, *Macromolecules*, 2008, **41**, 9736–9743.
26 A. Cravino, *Polym. Int.*, 2007, **56**, 943–956.
27 J. Roncali, *Chem. Soc. Rev.*, 2005, **34**, 483–495.
28 A. Cravino and N. S. Sariciftci, *J. Mater. Chem.*, 2002, **12**, 1931–1943.
29 L. Schmidt-Mende, A. Fechtenkotter, K. Mullen, E. Moons, R. H. Friend and J. D. MacKenzie, *Science*, 2001, **293**, 1119–1122.
30 A. M. Ramos, M. T. Rispens, J. K. J. van Duren, J. C. Hummelen and R. A. J. Janssen, *J. Am. Chem. Soc.*, 2001, **123**, 6714–6715.
31 B. de Boer, U. Stalmach, P. F. van Hutten, C. Melzer, V. V. Krasnikov and G. Hadziioannou, *Polymer*, 2001, **42**, 9097–9109.
32 P. A. van Hal, J. Knol, B. M. W. Langeveld-Voss, S. C. J. Meskers, J. C. Hummelen and R. A. J. Janssen, *J. Phys. Chem. A*, 2000, **104**, 5974–5988.
33 E. Peeters, P. A. van Hal, J. Knol, C. J. Brabec, N. S. Sariciftci, J. C. Hummelen and R. A. J. Janssen, *J. Phys. Chem. B*, 2000, **104**, 10174–10190.
34 A. Cravino, G. Zerza, M. Maggini, S. Bucella, M. Svensson, M. R. Andersson, H. Neugebauer and N. S. Sariciftci, *Chem. Commun.*, 2000, 2487–2488.
35 O. Wallquist and R. Lenz, *Macromol. Symp.*, 2002, **187**, 617–630.
36 Z. Hao and A. Iqbal, *Chem. Soc. Rev.*, 1997, **26**, 203–213.
37 P. Sonar, S. P. Singh, E. L. Williams, Y. Li, M. S. Soh and A. Dodabalapur, *J. Mater. Chem.*, 2012, **22**, 4425–4435.
38 A. V. Patil, W.-H. Lee, K. Kim, H. Park, I. N. Kang and S.-H. Lee, *Polym. Chem.*, 2011, **2**, 2907–2916.
39 S. Izawa, K. Hashimoto and K. Tajima, *Chem. Commun.*, 2011, **47**, 6365–6367.
40 T. L. Chen, Y. Zhang, P. Smith, A. Tamayo, Y. Liu and B. Ma, *ACS Appl. Mater. Interfaces*, 2011, **3**, 2275–2280.
41 H. Bronstein, Z. Chen, R. S. Ashraf, W. Zhang, J. Du, J. R. Durrant, P. Shakya Tuladhar, K. Song, S. E. Watkins, Y. Geerts,

M. M. Wienk, R. A. J. Janssen, T. Anthopoulos, H. Sirringhaus, M. Heeney and I. McCulloch, *J. Am. Chem. Soc.*, 2011, **133**, 3272–3275.
42 J. C. Bijleveld, B. P. Karsten, S. G. J. Mathijssen, M. M. Wienk, L. D. M. de and R. A. J. Janssen, *J. Mater. Chem.*, 2011, **21**, 1600–1606.
43 S. Loser, C. J. Bruns, H. Miyauchi, R. P. Ortiz, A. Facchetti, S. I. Stupp and T. J. Marks, *J. Am. Chem. Soc.*, 2011, **133**, 8142–8145.
44 P. Sonar, S. P. Singh, Y. Li, M. S. Soh and A. Dodabalapur, *Adv. Mater.*, 2010, **22**, 5409–5413.
45 T. L. Nelson, T. M. Young, J. Liu, S. P. Mishra, J. A. Belot, C. L. Balliet, A. E. Javier, T. Kowalewski and R. D. McCullough, *Adv. Mater.*, 2010, **22**, 4617–4621.
46 J. C. Bijleveld, V. S. Gevaerts, D. Di Nuzzo, M. Turbiez, S. G. J. Mathijssen, D. M. de Leeuw, M. M. Wienk and R. A. J. Janssen, *Adv. Mater.*, 2010, **22**, 242–246.
47 C. H. Woo, P. M. Beaujuge, T. W. Holcombe, O. P. Lee and J. M. J. Frechet, *J. Am. Chem. Soc.*, 2010, **132**, 15547–15549.
48 Y. Zou, D. Gendron, R. Neagu-Plesu and M. Leclerc, *Macromolecules*, 2009, **42**, 6361–6365.
49 E. Zhou, S. Yamakawa, K. Tajima, C. Yang and K. Hashimoto, *Chem. Mater.*, 2009, **21**, 4055–4061.
50 E. Zhou, Q. Wei, S. Yamakawa, Y. Zhang, K. Tajima, C. Yang and K. Hashimoto, *Macromolecules*, 2009, **43**, 821–826.
51 J. C. Bijleveld, A. P. Zoombelt, S. G. J. Mathijssen, M. M. Wienk, M. Turbiez, D. M. de Leeuw and R. A. J. Janssen, *J. Am. Chem. Soc.*, 2009, **131**, 16616–16617.
52 W. Kylberg, P. Sonar, J. Heier, J.-N. Tisserant, C. Muller, F. Nuesch, Z.-K. Chen, A. Dodabalapur, S. Yoon and R. Hany, *Energy Environ. Sci.*, 2011, **4**, 3617–3624.
53 B.-S. Jeong, H. Choi, N. Cho, H. M. Ko, W. Lim, K. Song, J. K. Lee and J. Ko, *Sol. Energy Mater. Sol. Cells*, 2011, **95**, 1731–1740.
54 A. B. Tamayo, X.-D. Dang, B. Walker, J. Seo, T. Kent and T.-Q. Nguyen, *Appl. Phys. Lett.*, 2009, **94**, 103301.
55 A. B. Tamayo, B. Walker and T.-Q. Nguyen, *J. Phys. Chem. C*, 2008, **112**, 11545–11551.
56 B. P. Karsten, R. K. M. Bouwer, J. C. Hummelen, R. M. Williams and R. A. J. Janssen, *Photochem. Photobiol. Sci.*, 2010, **9**, 1055–1065.
57 B. P. Karsten, P. P. Smith, A. B. Tamayo and R. A. J. Janssen, *J. Phys. Chem. A*, 2012, **116**, 1146–1150.
58 A. Lafleur-Lambert, S. Rondeau-Gagne, A. Soldera and J.-F. Morin, *Tetrahedron Lett.*, 2011, **52**, 5008–5011.
59 J. C. Hummelen, B. W. Knight, F. Lepeq, F. Wudl, J. Yao and C. L. Wilkins, *J. Org. Chem.*, 1995, **60**, 532–538.
60 C. Yang, J. K. Lee, A. J. Heeger and F. Wudl, *J. Mater. Chem.*, 2009, **19**, 5416–5423.
61 P. C. Beaumont, D. G. Johnson and B. J. Parsons, *J. Chem. Soc., Faraday Trans.*, 1993, **89**, 4185–4191.
62 N. Banerji, S. Cowan, M. Leclerc, E. Vauthey and A. J. Heeger, *J. Am. Chem. Soc.*, 2010, **132**, 17459–17470.
63 A. Morandeira, L. Engeli and E. Vauthey, *J. Phys. Chem. A*, 2002, **106**, 4833–4837.
64 C. J. Brabec, G. Zerza, G. Cerullo, S. De Silvestri, S. Luzzati, J. C. Hummelen and S. Sariciftci, *Chem. Phys. Lett.*, 2001, **340**, 232–236.
65 I.-W. Hwang, D. Moses and A. J. Heeger, *J. Phys. Chem. C*, 2008, **112**, 4350–4354.
66 K. G. Jespersen, F. L. Zhang, A. Gadisa, V. Sundstrom, A. Yartsev and O. Inganas, *Org. Electron.*, 2006, **7**, 235–242.